High yield extraction of oleosins, the proteins that plants developed to stabilize oil droplets

Lorenz Plankensteiner [a,b], Jack Yang [b], Johannes H. Bitter [b], Jean-Paul Vincken [a], Marie Hennebelle [a,**], Constantinos V. Nikiforidis [b,*]

[a] *Laboratory of Food Chemistry, Wageningen University, the Netherlands*
[b] *Laboratory of Biobased Chemistry and Technology, Wageningen University, the Netherlands*

ARTICLE INFO

ABSTRACT

Oleosins are unique proteins that are crucial for the stabilization of the oil droplets, that nature designed to store and protect triacylgycerols in seeds. To better understand and possibly replicate the role of oleosins in the stability of oil droplets, an efficient extraction for oleosins is necessary, which has not been achieved yet. Oleosins consist of a long central hydrophobic hairpin that is attached to two hydrophilic arms. This high amphiphilicity makes their extraction a challenging task. The aim of the present work was to develop a scalable method to extract oleosins from rapeseed oleosomes using washing steps with methanol, hexane, and ethanol (MHE). Following this method, we obtained oleosins with a recovery of 94 ± 1.4 wt% and a purity of 87.1 ± 1.9 wt%. The recovery was significantly higher ($p < 0.005$) compared to the commonly applied Folch extraction (recovery of 57.2 ± 5.5 wt%). Oleosins formed micro- and nanosized aggregates when dispersed in aqueous solutions, because of their long hydrophobic moiety. The fraction of nanosized aggregates was 6-fold higher for the oleosins obtained with the MHE method in comparison to those obtained using the Folch method. Due to the smaller aggregates, oleosins obtained using the MHE method were more efficient in reducing the oil-water interfacial pressure and formed a stronger interfacial film in comparison to those obtained with the Folch method. The highly efficient and scalable oleosin extraction, paves the way for elucidating the stabilizing role of oleosins and the way towards industrial oleosin extraction.

1. Introduction

Through evolution, nature designed sophisticated functional materials. Among them are oleosomes, oil droplets that nature designed to store and protect triacylglycerols in seeds (Nikiforidis, 2019). Oleosomes consist of a core of triacylglycerols (TAG), surrounded by an interfacial monolayer of phospholipids (PL) imbedded with structural proteins (Fig. 1), of which the main ones are oleosins (Huang, 2018; Jolivet et al., 2009).

The high physical and chemical stability of oleosomes has recently raised the interest to utilize them as natural oil droplets in emulsions for food, cosmetics and pharmaceuticals (Nikiforidis, 2019; Weiss & Zhang, 2020). Even after their aqueous extraction from seeds or nuts, oleosomes remain stable against coalescence. Furthermore, electrostatic repulsion prevents aggregation of oleosomes at pH's far away from their isoelectric point (~5–6) and at low ionic strength (<25 mM at pH 7) (Iwanaga

et al., 2007; Qi et al., 2017). Additionally, oleosomes were suggested to be relatively stable against lipid oxidation (Gray et al., 2010; Zaaboul et al., 2018). The high stability of oleosomes is, however, only provided after deactivation of the endogenous hydrolytic enzymes (De Chirico et al., 2020).

The mechanism behind the stability of oleosomes is still not fully known. Oleosins are suggested to play a key role (Huang & Huang, 2017), but little is known on the exact function of oleosins for the physical and oxidative stability of oleosomes. Oleosins are unique proteins with a triblock structure consisting of a long central hydrophobic hairpin (~72 residues) that is attached to a hydrophilic N-terminal arm and a hydrophilic C-terminal arm (Huang & Huang, 2017). It is believed that the anchoring of the hydrophobic hairpin into the lipid core is important for forming and stabilizing natural oleosomes (Huang & Huang, 2017; Jolivet et al., 2017). The arms are mostly polar and contain a mix of amino acids with positively and negatively charged side

---

* Corresponding author.
** Corresponding author.
E-mail addresses: marie.hennebelle@wur.nl (M. Hennebelle), costas.nikiforidis@wur.nl (C.V. Nikiforidis).

groups at the physiological pH of seeds (Jolivet et al., 2009; Wahlroos et al., 2015). The positively charged side groups are suggested to electrostatically interact with anionic phospholipids of the monolayer. The negatively charged side groups might be oriented towards the outer side of oleosomes and provide steric and electrostatic repulsion, preventing their coalescence and aggregation (Tzen et al., 1992; Tzen & Huang, 1992; Wahlroos et al., 2015). Further insights into the role of oleosins would increase the understanding of the mechanism behind the stability of oleosomes and possibly allow to replicate their function for nature-inspired oil droplets.

Studying the role of oleosins for the stability of oleosomes is not a trivial task, since oleosins must be extracted in sufficient quantity from plant sources directly or from microorganisms after biotechnological production. The simplest route to obtain oleosins is to extract them from abundant plant sources like oilseeds. Existing extraction methods focus on initially obtaining oleosomes, and subsequently purifying oleosins using a solvent mixture of methanol, chloroform and water, based on the lipid extraction method developed by Folch et al. (1957) (Tzen & Huang, 1992). Using this solvent mixture, a biphasic system is formed, where TAG and PL partition into the lower chloroform phase, while the amphiphilic oleosins need to be carefully collected from the interface (Tzen & Huang, 1992). This method is the foundation for most methods used to purify oleosins (Deleu et al., 2010; Nikiforidis et al., 2013; Pan et al., 2022). The most recent methods introduced a sonication pre-treatment of oleosomes and an additional washing step with acetone (Nikiforidis et al., 2013; Pan et al., 2022; Sun et al., 2022). Furthermore, there was little progress in oleosin extraction and limited data are available on the yield and recovery of this method. Only one recent study reported a recovery of 34–40% of oleosins from soybean oleosomes (Sun et al., 2022). This low recovery and the complicated procedure clearly highlight the need for new protocols to extract oleosins more efficiently.

In the present work, a new method using sequential washes of methanol, hexane, and ethanol (MHE) was developed, with the aim to efficiently extract larger amounts of oleosins from rapeseed oleosomes. The recovery, purity and functionality (in terms of solubility and interfacial activity) of the obtained oleosins was compared with oleosins obtained using the standard Folch method.

2. Materials and methods

2.1. Materials

Rapeseeds (*Brassica napus* L., variety Alizze) were purchased from a European seed producer and stored at −20 °C until use. Rapeseed oil was provided by Danone Nutricia Research (Utrecht, The Netherlands). All organic solvents were obtained from Biosolve (Valkenswaard, The Netherlands). Chemicals used for SDS PAGE were purchased from Bio-Rad (Veenendaal, The Netherlands). All other chemicals used in this study were sourced from Merck (Darmstadt, Germany. Milli-Q water (Merck, Darmstadt, Germany) was used for all aqueous solutions and dispersions.

2.2. Oleosome extraction

Oleosomes were extracted from rapeseeds by applying the method of De Chirico et al. (2018) with minor modifications. In short, rapeseeds were soaked in 0.1 M NaHCO$_3$ (pH 9.5) at a seed-to-solution ratio of 1:7 (w/w) for 16 h at 4 °C. The soaked mixture was ground in a laboratory blender (Waring Commercial 7011HS, Torrington, USA) for 2 min at maximum speed. The obtained slurry was filtered through a cheese cloth using a vacuum pump to remove seed solids. The resulting filtrate was centrifuged at 10,000×*g* for 30 min at 4 °C to separate oleosomes from other soluble seed materials. After centrifugation, the oleosome-rich top layer was carefully collected with a spatula. The collected material was further washed twice; first with 0.1 M NaHCO$_3$ solution (pH 9.5) and then with water, both at 1:4 (w/w) cream-to-solution ratio. Each washing step was followed by the same centrifugation and collection step as described earlier. The top layer collected after the final washing represented the oleosome cream and was stored at −30 °C until further use. The oleosome cream had a moisture content of ~60 wt%.

2.3. Oleosin isolation

The newly developed method that purified oleosins from the other oleosome constituents (PL and TAG) with methanol, hexane and ethanol (2.3.1) was compared to the Folch method (2.3.2).

2.3.1. Methanol, hexane and ethanol (MHE)

Oleosome cream (10 g) was mixed with 20 mL of methanol. Methanol disrupted the oleosome structure by dissolving PL out of the interfacial membrane. The solubility of oleosins and TAG in methanol is limited, which led to an oleosin pellet and an emerging TAG phase (Fig. 2). The mixture was incubated for 10 min at room temperature with occasional mixing and then centrifuged for 10 min at 4,700×*g*. After centrifugation, the top methanol phase was removed, and the pellet and TAG layer were collected. The washing was repeated three additional times with 20 mL methanol. Then, 20 mL hexane were added to the collected oleosin-TAG mixture and incubated for 10 min. The hexane dissolved TAG, which were separated from the precipitated
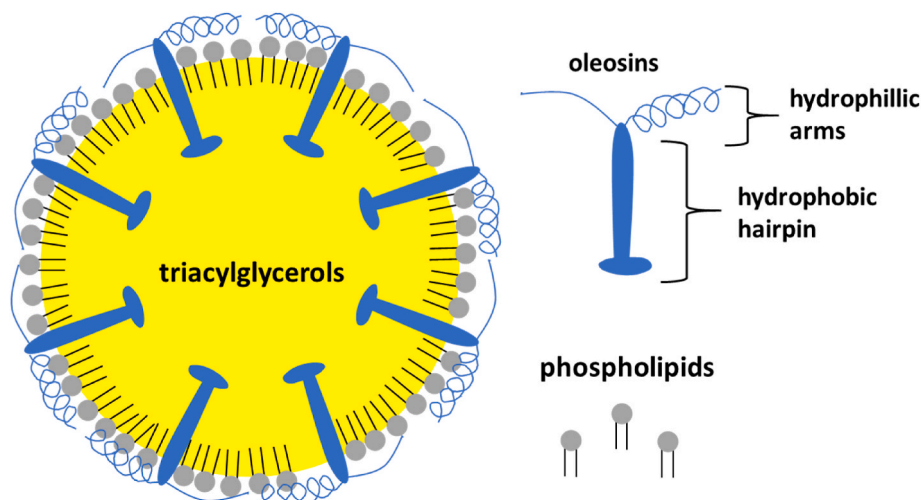

Fig. 1. Schematic structure of an oleosome and its main constituents. The illustrations are not to scale.
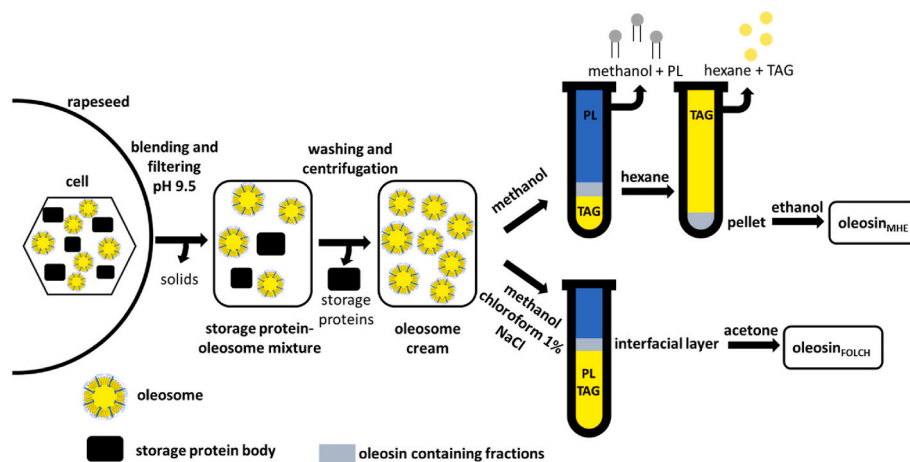
Fig. 2. Overview of the two different extraction processes, MHE and Folch, to obtain oleosins from rapeseed oleosomes. PL is used as abbreviation for phospholipids and TAG as abbreviation for triacylglycerols.

oleosins by centrifugation (10 min at 4,700×*g*). The same hexane washing was performed 3 additional times. The sequence of first using methanol and then hexane was crucial, as the methanol washings disrupted the oleosome structure, which made the TAG available for hexane extraction. Finally, residual lipids were removed with three washes of 10 mL ethanol (same incubation and centrifugation as for washes of methanol and hexane). The collected pellet was dispersed in 5 mL water by sonicating the mixture in a sonication bath (M2800 running at 40 kHz, Branson, Ferguson, USA) for 5 min. This mix was frozen and lyophilized resulting in oleosin$_{MHE}$. Oleosin$_{MHE}$ was stored at −30 °C until further use.

2.3.2. Methanol, chloroform and 1% NaCl (Folch)

Oleosome cream (10 g with moisture content of ~40%) was mixed with 20 mL chloroform, 10 mL methanol and 1 mL aqueous NaCl (1% w/w) to reach a final volume ratio of 4:2:1 chloroform-methanol-water (Nikiforidis et al., 2013). This mix was incubated for 10 min at room temperature with occasional mixing. The solvent mixture successfully dissolved both PL and TAG, rupturing the oleosome structure. Then, the mixture was centrifuged for 10 min at 4,700×*g*. After centrifugation, a biphasic system emerged with a white intermediate layer representing oleosin, as illustrated in Fig. 2. The top phase of this system was mainly methanol and water containing 1% NaCl, while the bottom phase was composed of chloroform and some methanol (<15%) (Eggers & Schwudke, 2016, pp. 1–6). TAG and most PL are predominantly non-polar and partitioned into the lower chloroform phase. Oleosins dissolved in neither of the phases, and accumulated at the interface (Nikiforidis et al., 2013; Tzen & Huang, 1992). From the interface, the oleosins were carefully collected and washed again with 20 mL chloroform, 10 mL methanol and 5 mL aqueous NaCl (1% w/w) followed by incubation and centrifugation. The interfacial layer containing the oleosins was collected. The collected material was washed three times with 5 mL of acetone to remove residual lipids (Nikiforidis et al., 2013). Each wash included an incubation of 10 min followed by centrifugation for 10 min at 4,700×*g*. Then, the pellet was collected and dried under nitrogen to remove remaining solvents. The remaining pellet was mixed with 5 mL water, frozen, and lyophilized, resulting in oleosin$_{FOLCH}$. Oleosin$_{FOLCH}$ was stored at −30 °C until further use.

2.4. Dry matter-, ash- and protein content

Dry matter content was determined gravimetrically after drying the samples overnight at 103 °C. The dried samples were then burned at 550 °C to determine the ash content gravimetrically. The protein content was determined with the Dumas method (FlashEA 1112 Series, Thermo

Scientific, Waltham, USA). A nitrogen-protein conversion factor of 5.7 was used, calculated from the amino acids sequence of oleosin S3, being one of the main oleosin isoforms present in rapeseed (Jolivet et al., 2009). The amino acid sequence of oleosin S3 was retrieved from Uniprot with the accession number C3S7G6. Protein purity was expressed as protein content on dry matter base.

2.5. Extraction recovery and purity of oleosins

The weight-based recovery and purity of oleosins from oleosomes were calculated according to equations (1) and (2).

$$oleosin\ recovery\ (wt\%) = \frac{g\ of\ proteins\ in\ oleosin\ extract}{g\ of\ proteins\ in\ oleosomes} \quad (1)$$

$$oleosin\ purity\ (wt\%) = \frac{g\ of\ proteins}{g\ of\ dry\ matter} \quad (2)$$

2.6. Protein compositional analysis

Oleosome cream (40–70 mg) or oleosins (1–2 mg) were dissolved in 1 mL aqueous SDS solution (2% w/w) for 15 min at 75 °C. The protein solutions were then mixed in a ratio of 1:2 v/v with Laemmli buffer (Bio-Rad, Veenendaal, The Netherlands) (non reducing conditions) or Laemmli buffer including 100 mM dithiothreitol (reducing conditions), and incubated for 15 min at 95 °C. Proteins were resolved using Mini-Protean TGX gels (4–20%) (Bio-Rad) run in a Mini-Protean II system (Bio-Rad) according to the manufacturer's protocol at 100 V. The Precision Plus™ Protein standard (Bio-Rad) was used as a molecular weight marker (10–250 kDa). After electrophoresis, the gels were washed with water and stained with comassie brilliant blue R-250. Finally, gels were analyzed with a gel scanner (GS-900, Bio-Rad).

2.7. Transmission Electron Microscopy (TEM)

Oleosins were dispersed in water at a concentration of 1 g/L. The dispersions were shaken for 1 h at room temperature and then sonicated for 10 min in a sonication bath (CPX 2800 running at 40 kHz, Branson, Ferguson, USA). Aliquots of 6 μL were pipetted onto a carbon-coated hexagonal 400 mesh copper grid. After 1 min, filter paper was used to remove excess fluid, and the sample was stained with 6 μl of 2% phosphotungstic acid (pH 6.8). A minute after staining, again a filter paper was used to remove excess fluid. Then, the sample was air dried and imaged with a JEOL JEM1400+ microscope (JEOL Ltd., Tokyo, Japan) operating at 120 kV. Sizes of the protein aggregates were estimated by measuring the diameters of aggregates with the software FIJI

(Schindelin et al., 2012).

2.8. Molecular and interfacial properties

To measure the molecular and interfacial properties of the different oleosin isolates, oleosins were dispersed at a concentration of 1 g/L in 10 mM phosphate buffer at pH 8. The ionic strength was adjusted to 30 mM with NaCl. The dispersions were shaken for 1 h at room temperature and then sonicated for 10 min in a sonication bath (running at 40 kHz).

2.8.1. Protein content in solution, particle size and ζ-potential

The sonicated oleosin samples were filtered through a 0.45 μm filter (Minisart® Cellulose-Acetate, Sartorius, Göttingen, Germany) to remove microsized aggregates which otherwise would hinder the measurements. The protein content in the filtrate was measured with the Pierce™ BCA protein assay kit (Thermo Scientific, Waltham, USA). The particles size was determined by measuring intensity averaged hydrodynamic diameter (z-average) and the polydispersity index (PDI) with a Zetasizer Nano ZS (Malvern Instruments, Worcestershire, UK). The ζ-potential of oleosins in the filtrate were as well measured with the Zetasizer Nano ZS. The refractive index of water of 1.33 was used for the dispersant, and 1.45 was used as refractive index for the oleosins according to the manufacturer's guidelines for proteins. Measurements were performed at 22 °C and the results were collected as averages of three sequential measurement runs.

2.8.2. Interfacial properties

Interfacial adsorption and dilatational rheological properties of oleosins at the oil-water interface were studied with an automated drop tensiometer (ADT) (Teclis, Lyon, France). Rapeseed oil stripped from interfacial active impurities was used as oil phase. For the stripping, rapeseed oil and Florisil (100–200 mesh, magnesium silicate, Merck, Darmstadt, Germany) were mixed in a ratio of 2:1 (v/v), covered in aluminum foil and shaken overnight at room temperature. This mixture was then centrifuged three times at 2,000×g for 20 min to remove the Florisil. The stripped oil was stored at −20 °C until use.

A pendant drop (interfacial area of 30 mm^2) of oleosin dispersion (1 g/L) was created on the tip of a coated G18 needle immersed in the stripped rapeseed oil. Additionally, the fraction containing nanosized oleosin aggregates was separately studied after filtration of the dispersions through a 0.45 μm filter. The droplet was monitored by a camera, and the shape was fitted to the Young-Laplace equation to determine the interfacial tension. The difference of interfacial tension of the interface in absence and presence of oleosins was expressed as interfacial pressure. After keeping the droplet area constant for 2 h, amplitude sweeps were performed with a constant frequency of 0.02 Hz. The droplet area was compressed and expanded with deformations ranging from 2.5 to 50.0%. At each deformation amplitude, five oscillatory cycles were performed with a 50 s pause between each deformation step. The oscillating interfacial tension signals were Fourier transformed, and the intensity and phase of the first harmonic was used to calculate the dilatational elastic modulus (E_d') and the dilatational viscous modulus (E_d'').

$$E_d' = \Delta\gamma \left(\frac{A_0}{\Delta A}\right)\cos\delta \quad (3)$$

$$E_d'' = \Delta\gamma \left(\frac{A_0}{\Delta A}\right)\sin\delta \quad (4)$$

where $\Delta\gamma$ is the difference between the interfacial tension before and after deformation, A_0 the initial droplet area, ΔA the change in area, and δ the phase shift between oscillating interfacial tension signal and induced area change. All experiments were performed at 20 °C.

2.9. Statistical analysis

Independent t-tests were performed with the software SPSS (v25.0, IBM, Armonk, USA) to compare recovery, purity, and functional properties of oleosin$_{FOLCH}$ and oleosin$_{MHE}$ at the 5% significance level. All extractions and measurements were performed in triplicate.

3. Results and discussion

3.1. Oleosome extraction

An overview of the new MHE- and the commonly used Folch extraction is given in Fig. 2. The first step for both oleosin extractions was to isolate intact oleosomes from storage proteins and other seed materials. Oleosomes have a hydrophilic surface that has a high negative charge at alkaline pH, which was used to extract them with an aqueous extraction method (De Chirico et al., 2018).

The extracted oleosomes had a protein content of 2.6 ± 0.1% on dry matter. This low protein content indicated that oleosomes were free of storage proteins (De Chirico et al., 2018). The separation of storage proteins was further confirmed with SDS-PAGE (Fig. 3). On the SDS-PAGE gel, a main band at 17 kDa and faint bands at 20 kDa and 25 kDa were present. The main band at 17 kDa, and the faint band at 20 kDa were tentatively assigned to oleosins, while the faint band at 25 kDa was assigned to caleosins (Jolivet et al., 2009, 2011). To ensure that oleosins were responsible for the main band, the gels were additionally run under reducing conditions. Oleosins and the rapeseed storage protein napin have a comparable molecular weight (Ntone et al., 2020). However, in contrast to oleosins, napin proteins are constituted of different subunits that are crosslinked with disulfide bonds. These disulfide bonds break under reducing conditions, making napins appear as their subunits with molecular weights of 5–11 kDa (Ntone et al., 2020). No smaller bands appeared under reducing conditions confirming that oleosins were the main proteins of the extracted oleosomes.

At the alkaline extraction conditions, oleosomes and seed storage proteins electrostatically repelled each other, due to their negatively charged interface (De Chirico et al., 2018; Weiss & Zhang, 2020), leading to a successful separation of storage proteins and oleosomes. Having pure oleosomes as starting material is of major importance, as storage proteins would otherwise be coextracted during the following oleosin extraction (data not shown).

3.2. Oleosin extraction

Oleosins were further purified from the two other main components of oleosomes, PL and TAG. The extracted oleosin$_{MHE}$ had a protein purity of 87.1 ± 1.9%. The protein composition was investigated with SDS-PAGE (Fig. 3). Like for the oleosomes, a main band at 17 kDa was detected and a faint band at 20 kDa, which were representing oleosins. Five different oleosin isoforms are known to be present in rapeseed oleosomes called oleosin S1–S5 (Jolivet et al., 2009). The isoforms oleosin S1–S3 were reported to be the most abundant oleosins, composing ~85% of the oleosins in rapeseed. The molecular weight of oleosin S1–S3 are very similar and usually not fully resolved with SDS-PAGE (Jolivet et al., 2009, 2013). Oleosin S4 has a slightly higher molecular weight and comprises ~13%. The smallest and least abundant is oleosin S5, being ~2% of the oleosins in rapeseed (Jolivet et al., 2009). Based on these previous results, the main band on our gel at 17 kDa most likely represented a combination of oleosins S1–S3, while the band at 20 kDa most likely corresponded to oleosin S4 (Jolivet et al., 2009). The abundance of oleosin S5 was probably too low to be detected. This showed that the extracted oleosins were a mix of different oleosin isoforms.

The comparison of the extraction efficiency of the MHE method to the commonly used Folch method highlighted the advantages of the new MHE method (Table 1). Remarkably, the recovery of oleosins with the
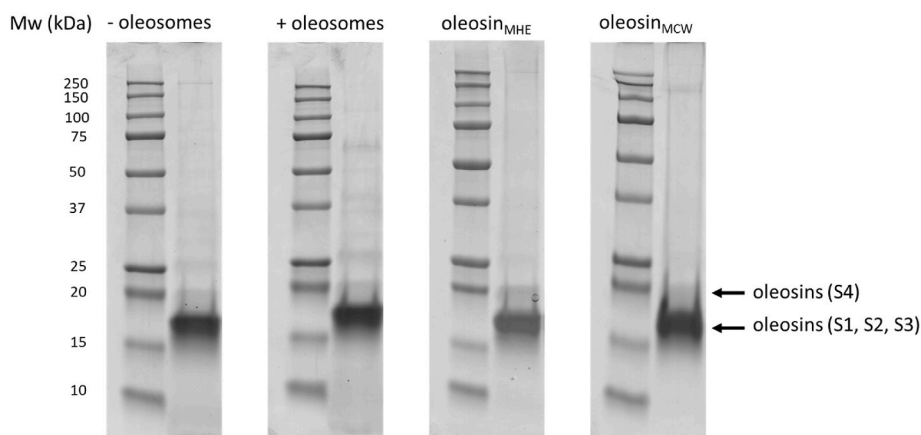
Fig. 3. SDS PAGE gels of oleosomes under non reducing (−) and reducing (+) conditions, oleosin$_{MHE}$ and oleosin$_{FOLCH}$. On each gel, the first lane corresponds to the molecular weight marker and the second lane to the corresponding sample. Arrows indicate bands that were assigned to the different oleosin isoforms.

Table 1
Recovery, purity and concentration of nanosized oleosins aggregates in solution for oleosins extracted with methanol, hexane and ethanol (MHE) or with methanol, chloroform and 1% NaCl (Folch). Letters in superscript indicate significant differences (*t*-test; p < 0.05) between the two extraction methods, MHE and Folch.

Extraction Method	Recovery (wt %)	Purity (wt %)	Nanosized oleosin aggregates in solution (g/L)
MHE	94.4 ± 1.4[a]	87.1 ± 1.9[a]	0.17 ± 0.03[a]
Folch	57.2 ± 5.5[b]	85.5 ± 1.6[a]	0.03 ± 0.00[b]

MHE method was almost 95 wt%. This recovery was significantly (*p* < 0.005) higher than the 57 wt% obtained with the Folch method (Table 1), and much higher than the 34–40% that were reported for soybean oleosins (Sun et al., 2022). The protein composition (Fig. 3) of oleosin$_{MHE}$ and oleosin$_{FOLCH}$ was almost identical, both consisting mainly of oleosins with a molecular weight of ~17 kDa. In addition, no significant differences were observed in protein purity between oleosin$_{MHE}$ and oleosin$_{FOLCH}$, both being ~85% pure (Table 1). Both oleosin extracts contained minor inorganic impurities shown by the ash contents of 1.9 wt% and 2.7 wt% for oleosin$_{MHE}$ and oleosin$_{FOLCH}$, respectively.

The new MHE method showed great potential for upscaling; 10 g of oleosins were extracted in less than a week and further scaling would be possible with the right equipment. Achieving such large quantities with the Folch method is almost impossible, as it is far from easy to collect oleosins from the interface of the biphasic solvent system at a larger scale. The MHE method is a simple and scalable extraction process that yields a high oleosin recovery while maintaining oleosin purity. Although the method was developed for research purposes, it can also be adapted to industry, after ensuring that the solvent residues in the oleosin extract are below the legal limits for the corresponding industry.

3.3. Molecular properties of oleosins in solution

In addition to a high extraction yield, the functional properties of the oleosins should be retained upon extraction. Consequently, we studied the molecular and oil-water interfacial properties of the extracted oleosins. When dispersed in water, oleosin$_{MHE}$ and oleosin$_{FOLCH}$ formed turbid solutions indicating aggregation of oleosins with some visible precipitate. The aggregates were analyzed with Transmission Electron Microscopy (TEM) to image them and to estimate their size. The aggregates were irregularly shaped particles ranging from 0.1 μm to 30 μm for both oleosins as visible in the TEM images in Fig. 4a and b and the additional TEM images in the supplemental information.

To test if monomeric oleosin molecules were also present, and to measure the charge of oleosins in solution, microsized oleosin aggregates were then removed by filtering through a 0.45 μm filter. Dynamic light scattering (DLS) was used to measure the hydrodynamic diameter and zeta potential of the nanosized oleosin aggregates in the filtrate. The charge of the two oleosin extracts was identical with a zeta potential of −9 mV. Also, the size distribution (Fig. 4c), the z-average diameter, and the polydispersity index (PDI) for both oleosins were similar, with a z-average of 205–209 nm and a PDI of 0.18–0.19, respectively. These results suggested the absence of monomeric oleosins, rather oleosins were present as nanosized aggregates with slight polydispersity. The fraction of oleosins that assembled into these nanosized aggregates was determined by measuring the protein content in the filtrate (Table 1). Nanosized aggregates comprised 20% of the total dispersed oleosin$_{MHE}$, which was more than 6 times higher than for oleosin$_{FOLCH}$ (only 3%).

Oleosins aggregated as soon as they were dispersed in aqueous solutions, forming micro- (>450 nm) and nanosized (<450 nm) aggregates. The unique triblock structure of oleosins is designed to stabilize the oil-water interface of oleosomes. The ~5–6 nm long central hairpin is highly hydrophobic and penetrates into the TAG core of oleosomes (Huang & Huang, 2017; Jolivet et al., 2017). When oleosins are removed from their native environment and dispersed in aqueous solution, this hydrophobic hairpin is exposed. Contact of the hydrophobic hairpin with water is energetically highly unfavorable and drives the aggregation of oleosins (Gohon et al., 2011; Vargo et al., 2012). Previous studies reported the structure of oleosin aggregates can be tuned by changing the properties of the hydrophilic arms that border the hairpin. Vargo et al. (2012) created different supramolecular assemblies like vesicles, sheets or fibers by truncating the hydrophilic arms of recombinant oleosins or by changing the ionic strength of the solvent. Therefore, the differences in the aggregate sizes between oleosin$_{MHE}$ and oleosin$_{FOLCH}$ likely derived from alterations in the structure of the hydrophilic arms. The combination of methanol and relatively high ionic strength (~0.2 M) in the top phase of the Folch extraction, probably decreased the interaction between the hydrophilic arms and the surrounding solvent (Zhou & Pang, 2018). This promoted the formation of more microsized aggregates for oleosin$_{FOLCH}$.

3.4. Interfacial properties

In general, aggregation is undesirable, as large aggregates might precipitate out of solution decreasing the functionality of oleosins. To overcome aggregation, chaotropes (Roux et al., 2004), amphipols or detergents (Gohon et al., 2011; Kim et al., 2007) were previously used, which increased the solubility of oleosins. However, these cosolvents are undesired when studying the interfacial properties of oleosins, as they
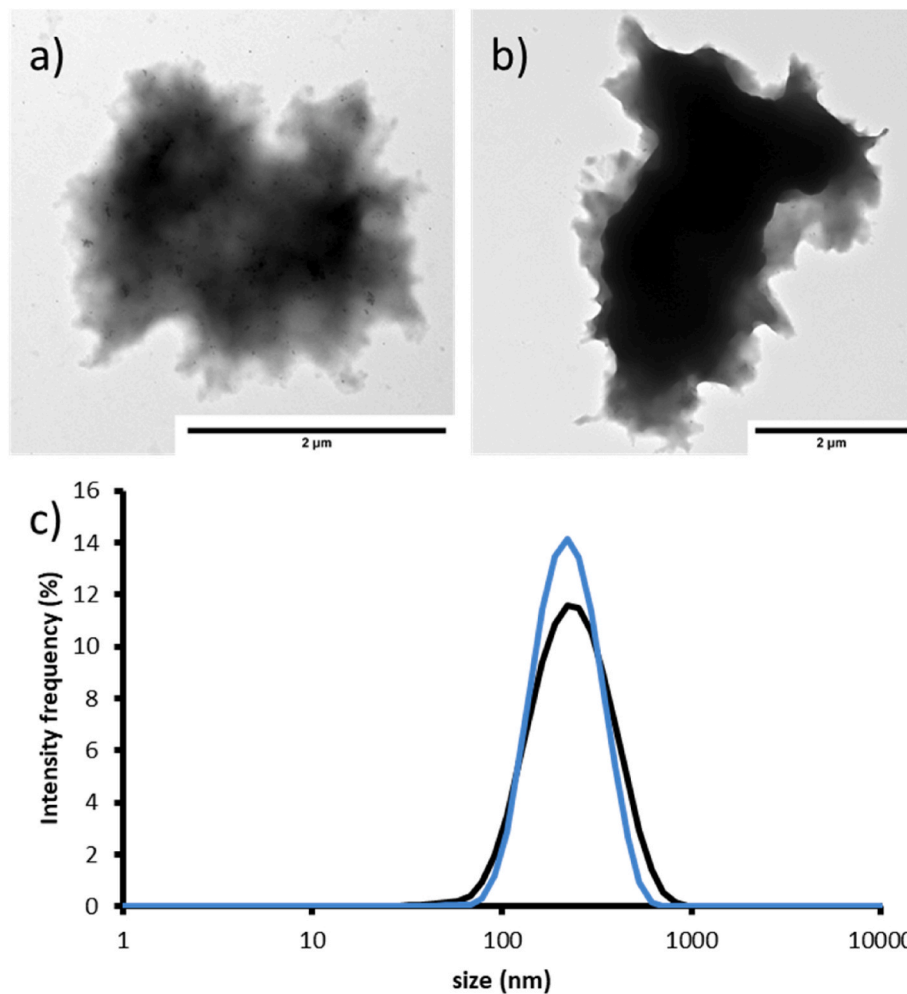
Fig. 4. Transmission electron microscopy (TEM) of microsized aggregates of oleosin$_{MHE}$ (a) and oleosin$_{FOLCH}$ (b) in water. Scale bars are visible at the right bottom of each image and show a distance of 2 μm. c) Size distributions of nanosized oleosin aggregates obtained after filtration, in black oleosin$_{MHE}$ and in blue oleosin$_{FOLCH}$. Data are plotted as mean (n=3). (For interpretation of the references to color in this figure legend, the reader is referred to the Web version of this article.)

will also adsorb onto the interface, thus influencing the analysis. In the present study, a different strategy was used. The interfacial properties of oleosins at the oil-water interface were studied by using aggregated oleosins. As oleosin aggregates are held together by the hydrophobic effect, we hypothesized that they would dissociate at the oil-water interface, and oleosins would spread at the interface to minimize the free energy of the system.

3.4.1. Interfacial adsorption

Oleosins were dispersed in an aqueous buffer at pH 8, and a pendant drop of this dispersion was created in oil. The interfacial adsorption was then monitored by measuring the evolution of the interfacial pressure over time (Fig. 5a). Oleosin$_{MHE}$ adsorbed immediately and rapidly increased the interfacial pressure to 8 mN/m after 15 s followed by a slower increase to reach an interfacial pressure of 15 mN/m after 2 h
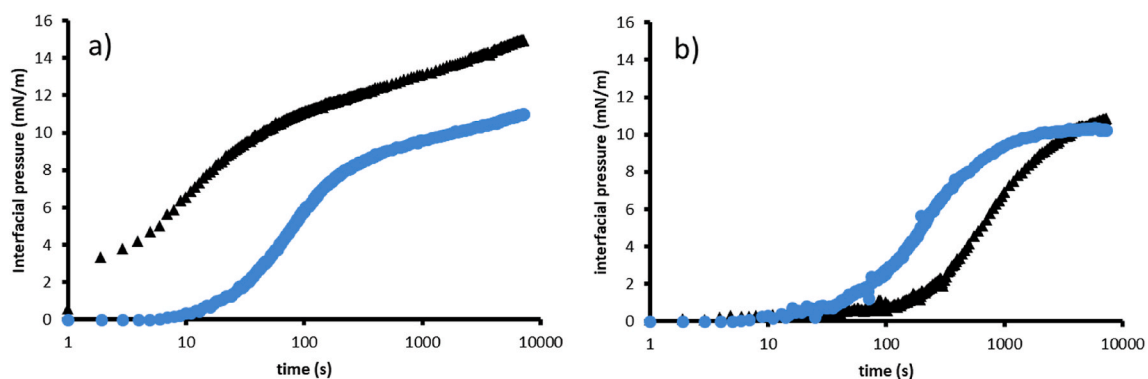

Fig. 5. Interfacial pressure as a function of time for oleosin$_{MHE}$ (▲) and oleosin$_{FOLCH}$ (●) stabilized oil-water interfaces measured with automated drop tensiometry (ADT). a) Dispersions containing micro- and nanosized aggregates (concentration= 1 g/L). b) Filtrates containing only nanosized aggregates (concentration=0.03 g/L). Data are plotted as mean (n=3).

(Fig. 5a). In contrast to oleosin$_{MHE}$, an induction period of 10 s was observed for oleosin$_{FOLCH}$, during which the interfacial pressure stayed constant (<2 mN/m). After this induction period, the surface pressure increased to reach 8 mN/m after 130 s (Fig. 5a). The increase then slowed down, resulting in an interfacial pressure of 12.3 mN/m after 2 h.

These results confirmed that oleosins can adsorb to the interface, even though they were present as micro- and nanosized oleosin aggregates in the aqueous phase. The rapid increase of the interfacial pressure was comparable to other proteins, such as whey and pea proteins (Hinderink et al., 2020). The high interfacial activity of oleosins is most likely based on their high hydrophobicity (Delahaije et al., 2014). To further test if aggregates of all sizes were interfacially active, oleosin dispersions were filtered through a 0.45 μm filter to remove the microsized aggregates and then remeasured with ADT. The interfacial pressure curves for the nanosized aggregates (data not shown) of oleosin$_{MHE}$ and oleosin$_{FOLCH}$ perfectly overlapped with the curves of the unfiltered dispersions (containing micro-and nanosized aggregates). These observations indicated that only nanosized aggregates (<450 nm) were interfacially active and responsible for the increase in interfacial pressure under the diffusion-controlled conditions in the ADT. Most likely, the microsized aggregates precipitated, and were not able to adsorb to the interface (Sagis & Scholten, 2014).

The interfacial adsorption of the nanosized aggregates of oleosin$_{MHE}$ (<450 nm) was comparable to previously investigated recombinant oleosins S3, which increased the interfacial pressure at a sunflower oil-water interface to 8.3 mN/m after 10 s and arrived at a pressure of 17.7 mN/m after 2 h, when dissolved in urea (Roux et al., 2004). This indicated that the oleosin aggregates may disassemble at the interface to give a similar interfacial activity as fully dissolved oleosins (in urea). However, the exact structure of the oleosin interfaces is still unknown. It is not yet completely clear if the oleosin interfaces are stabilized by monomeric oleosins or by nanosized oleosin aggregates. Investigating the exact structure of the interfacial layer of extracted oleosins would be essential for future studies.

The oleosin$_{MHE}$ filtrate was then diluted to the same concentration of nanosized aggregates as the filtrate of oleosin$_{FOLCH}$, to investigate if the amount of nanosized aggregates was responsible for the difference in adsorption. As a result, the interfacial pressure curves of both oleosins became more comparable (Fig. 5b). The diluted oleosin$_{MHE}$ adsorbed slightly slower than oleosin$_{FOLCH}$ in the first 4000 s, but finally reached the same interfacial pressure. This slightly slower adsorption of oleosin$_{MHE}$ might be related to small variations in protein concentration, due to potential inaccuracies of the BCA assay at such low concentrations. These results highlighted that the faster adsorption and higher interfacial pressure of oleosin$_{MHE}$ compared to oleosin$_{FOLCH}$ was derived from the six times higher amount of nanosized aggregates.

In summary, the nanosized aggregates of oleosin$_{FOLCH}$ and oleosin$_{MHE}$ had a similar size, structure (3.3) and interfacial activity. The amount of nanosized aggregates was higher for oleosin$_{MHE}$ providing a faster interfacial adsorption and higher interfacial pressure compared to oleosin$_{FOLCH}$.

3.4.2. Interfacial dilatational rheology

After an adsorption time of 2 h, interfacial dilatational amplitude sweeps were performed to determine the elastic (E_d') and viscous modulus (E_d'') of the oleosin interfaces. E_d' and E_d'' were calculated for different deformation amplitudes (2.5–50%) for oleosin dispersions (containing micro- and nanosized aggregates) (Fig. 6a) and the filtrates (only nanosized aggregates) that were corrected for the concentration of nanosized aggregates (Fig. 6b). For the dispersion of oleosin$_{MHE}$, the E_d' was substantially higher than E_d'', which is typical for viscoelastic interfaces. In addition, the E_d' was strongly amplitude dependent. The E_d' of oleosin$_{MHE}$ was 33.5 mN/m at a deformation amplitude of 2.5% and then almost halved to 16.5 mN/m at 50% deformation. In comparison, the E_d' for oleosin$_{FOLCH}$ was lower until a deformation of 30% and less dependent of the deformation amplitude. The E_d' of oleosin$_{FOLCH}$ changed from 20.9 mN/m at 2.5% deformation to 15.5 mN/m at 50% deformation.

The strong amplitude dependency for the E_d' of oleosin$_{MHE}$ was a clear indicator for the presence of a non-linear viscoelastic (NLVE) regime. In the NLVE regime, the E_d' is dependent on the applied strain and cannot be interpreted by solely looking at its value (Sagis & Fischer, 2014; Yang et al., 2022). The combination of substantially lower E_d'' compared to E' and the strain dependence of E_d' indicated that oleosin$_{MHE}$ formed a solid-like interface (Yang et al., 2022). The interfacial structure of the oleosin$_{MHE}$ disrupted at higher deformations. Most likely, oleosins formed a network through in-plane interactions, which led to a stiffness that was comparable to a whey protein stabilized interface (Hinderink et al., 2020). The pH 8 of the used buffer was close to the theoretical isoelectric point (IEP) of rapeseed oleosins, which varies between 7 and 10 for the different oleosin isoforms (Jolivet et al., 2009). This led to a low net charge of the oleosin arms, as highlighted by the relatively low zeta potential that was measured (section 3.3). The low charge likely promoted intermolecular interactions of oleosins at the interface.

The dispersion of oleosin$_{MHE}$ was then filtered and diluted to reach the same concentration of nanosized aggregates in solution as oleosin$_{FOLCH}$. The concentration corrected oleosin$_{MHE}$ had an E_d' of 19.4 mN/m at a deformation of 2.5%, which only slightly decreased to 14.2 mN/m at 50% deformation. The E_d' for the filtered oleosin$_{FOLCH}$ started at 16.9 mN/m at low deformation and then halved to 8.2 mN/m at 50% deformation. The filtered and diluted oleosin$_{MHE}$ had a weaker interface and the E_d' was less amplitude dependent compared to the undiluted dispersion. The interface of oleosin$_{MHE}$ was slightly stronger than the interface of filtered oleosin$_{FOLCH}$ as evidenced by the higher E_d'.

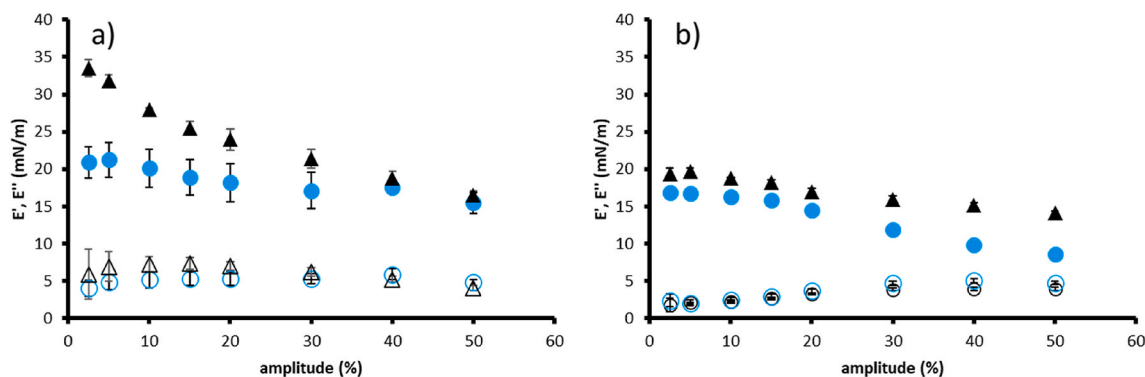The presence of a stiff interface only for the dispersion of oleosin$_{MHE}$

Fig. 6. Surface dilatational storage (E') modulus (filled symbols) and loss (E'') modulus (open symbols) as a function of deformation amplitude for the interfacial films stabilized by oleosin$_{MHE}$ (▲) and oleosin$_{FOLCH}$ (●). a) Dispersions containing micro- and nanosized aggregates of oleosins (concentration= 1 g/L). b) Filtrates containing only nanosized aggregates (concentration=0.03 g/L). Data are plotted as mean ± SD (n=3).

suggested that a minimum amount of oleosins at the interface is required to form in plane interactions. With the same concentration of nanosized aggregates (Fig. 6b), the oleosin$_{FOLCH}$ formed slightly weaker interfaces as oleosin$_{MHE}$. The weaker interface of oleosin$_{FOLCH}$ could have originated from a difference in charge, protein structure or aggregate state (Sagis & Scholten, 2014). The charge state of both oleosins was similar (section 3.3) and may not explain the observed differences in strength of the interface. Rather, alterations in the protein interactions might have led to the weaker interface of oleosin$_{FOLCH}$. We hypothesized these alterations occurred in the hydrophilic arms. The alterations most likely created the larger aggregates of oleosin$_{FOLCH}$, as shown in section 3.3, and the slightly weaker interface of oleosin$_{FOLCH}$.

4. Conclusions

The new oleosin extraction method using methanol, hexane and ethanol (MHE) recovers almost 95 wt% of oleosins from oleosomes. The recovery is substantially higher than the 57 wt% with the Folch method, while the same oleosin purity of ~85% is maintained. Extracted oleosins aggregate when dispersed in an aqueous buffer at pH 8. The size of these aggregates varies from 100 nm up to several μm and can be separated into micro- (>450 nm) and nanosized aggregates (<450 nm). The nanosized oleosin aggregates rapidly adsorb to and stabilize an oil-water interface by forming a solid-like interfacial layer. Oleosins extracted with the MHE method form more of these nanosized aggregates, and hence, are more functional than oleosins extracted with the Folch method. The MHE method has the potential to extract large amounts of oleosins which can be used to study the role of oleosins for the stability of oleosomes. Additionally, the method is an important step towards industrial oleosin extraction.

Author statement

Lorenz Plankensteiner: Funding acquisition; Conceptualization; Methodology; Investigation; Formal analysis; Writing – Original Draft. **Jack Yang:** Methodology; Investigation; Formal analysis; Writing – review & editing. **Johannes H. Bitter**: Writing – review & editing. **Jean-Paul Vincken:** Writing – review & editing. **Marie Hennebelle:** Funding acquisition; Conceptualization, Supervision, Writing – review & editing. **Constantinos V. Nikiforidis:** Funding acquisition; Conceptualization, Supervision, Writing – review & editing.

Declaration of competing interest

The authors declare that no competing interest existed.

Data availability

Data will be made available on request.

Acknowledgments

The authors thank Laura Schijven for collecting the TEM images. This research was funded by the Dutch Research Council (NWO) in the framework of the Green Top Sector Graduate School (GSGT.2019.021) and in collaboration with BOTANECO®.

Appendix A. Supplementary data

Supplementary data to this article can be found online at https://doi.org/10.1016/j.foodhyd.2022.108419.

References

De Chirico, S., di Bari, V., Foster, T., & Gray, D. (2018). Enhancing the recovery of oilseed rape seed oil bodies (oleosomes) using bicarbonate-based soaking and grinding media. *Food Chemistry, 241*, 419–426.
De Chirico, S., di Bari, V., Guzmán, M. J. R., Nikiforidis, C. V., Foster, T., & Gray, D. (2020). Assessment of rapeseed oil body (oleosome) lipolytic activity as an effective predictor of emulsion purity and stability. *Food Chemistry, 316*, Article 126355.
Delahaije, R. J., Gruppen, H., Giuseppin, M. L., & Wierenga, P. A. (2014). Quantitative description of the parameters affecting the adsorption behaviour of globular proteins. *Colloids and Surfaces B: Biointerfaces, 123*, 199–206.
Deleu, M., Vaca-Medina, G., Fabre, J.-F., Roïz, J., Valentin, R., & Mouloungui, Z. (2010). Interfacial properties of oleosins and phospholipids from rapeseed for the stability of oil bodies in aqueous medium. *Colloids and Surfaces B: Biointerfaces, 80*(2), 125–132.
Eggers, L., & Schwudke, D. (2016). *Liquid extraction: Folch*. Encyclopedia of lipidomics.
Folch, J., Lees, M., & Stanley, G. S. (1957). A simple method for the isolation and purification of total lipides from animal tissues. *Journal of Biological Chemistry, 226*(1), 497–509.
Gohon, Y., Vindigni, J.-D., Pallier, A., Wien, F., Celia, H., Giuliani, A., Tribet, C., Chardot, T., & Briozzo, P. (2011). High water solubility and fold in amphipols of proteins with large hydrophobic regions: Oleosins and caleosin from seed lipid bodies. *Biochimica et Biophysica Acta (BBA) - Biomembranes, 1808*(3), 706–716.
Gray, D. A., Payne, G., McClements, D. J., Decker, E. A., & Lad, M. (2010). Oxidative stability of Echium plantagineum seed oil bodies. *European Journal of Lipid Science and Technology, 112*(7), 741–749.
Hinderink, E. B., Sagis, L., Schroën, K., & Berton-Carabin, C. C. (2020). Behavior of plant-dairy protein blends at air-water and oil-water interfaces. *Colloids and Surfaces B: Biointerfaces, 192*, Article 111015.
Huang, A. H. (2018). Plant lipid droplets and their associated proteins: Potential for rapid advances. *Plant Physiology, 176*(3), 1894–1918.
Huang, C.-Y., & Huang, A. H. (2017). Unique motifs and length of hairpin in oleosin target the cytosolic side of endoplasmic reticulum and budding lipid droplet. *Plant Physiology, 174*(4), 2248–2260.
Iwanaga, D., Gray, D. A., Fisk, I. D., Decker, E. A., Weiss, J., & McClements, D. J. (2007). Extraction and characterization of oil bodies from soy beans: A natural source of pre-emulsified soybean oil. *Journal of Agricultural and Food Chemistry, 55*(21), 8711–8716.
Jolivet, P., Aymé, L., Giuliani, A., Wien, F., Chardot, T., & Gohon, Y. (2017). Structural proteomics: Topology and relative accessibility of plant lipid droplet associated proteins. *Journal of Proteomics, 169*, 87–98.
Jolivet, P., Boulard, C., Bellamy, A., Larré, C., Barre, M., Rogniaux, H., d'Andréa, S., Chardot, T., & Nesi, N. (2009). Protein composition of oil bodies from mature Brassica napus seeds. *Proteomics, 9*(12), 3268–3284.
Jolivet, P., Boulard, C., Bellamy, A., Valot, B., d'Andréa, S., Zivy, M., Nesi, N., & Chardot, T (2011). Oil body proteins sequentially accumulate throughout seed development in Brassica napus. *Journal of Plant Physiology, 168*(17), 2015–2020.
Jolivet, P., Deruyffelaere, C., Boulard, C., Quinsac, A., Savoire, R., Nesi, N., & Chardot, T. (2013). Deciphering the structural organization of the oil bodies in the Brassica napus seed as a mean to improve the oil extraction yield. *Industrial Crops and Products, 44*, 549–557.
Kim, H., Kim, S.-Y., Han, N. S., & Tao, B. Y. (2007). Solubilization conditions for hydrophobic membrane protein, oleosin, in soybeans. *Biotechnology and Bioprocess Engineering, 12*(5), 542–547.
Nikiforidis, C. V. (2019). Structure and functions of oleosomes (oil bodies). *Advances in Colloid and Interface Science, 274*, Article 102039.
Nikiforidis, C. V., Ampatzidis, C., Lalou, S., Scholten, E., Karapantsios, T. D., & Kiosseoglou, V. (2013). Purified oleosins at air–water interfaces. *Soft Matter, 9*(4), 1354–1363.
Ntone, E., Bitter, J. H., & Nikiforidis, C. V. (2020). Not sequentially but simultaneously: Facile extraction of proteins and oleosomes from oilseeds. *Food Hydrocolloids, 102*, Article 105598.
Pan, Y., Jin, W., & Huang, Q. (2022). Structure, assembly and application of novel peanut oil body protein extracts nanoparticles. *Food Chemistry, 367*, Article 130678.
Qi, B., Ding, J., Wang, Z., Li, Y., Ma, C., Chen, F., Sui, X., & Jiang, L. (2017). Deciphering the characteristics of soybean oleosome-associated protein in maintaining the stability of oleosomes as affected by pH. *Food Research International, 100*, 551–557.
Roux, É., Baumberger, S., Axelos, M. A., & Chardot, T. (2004). Oleosins of Arabidopsis thaliana: Expression in Escherichia coli, purification, and functional properties. *Journal of Agricultural and Food Chemistry, 52*(16), 5245–5249.
Sagis, L. M., & Fischer, P. (2014). Nonlinear rheology of complex fluid–fluid interfaces. *Current Opinion in Colloid & Interface Science, 19*(6), 520–529.
Sagis, L. M., & Scholten, E. (2014). Complex interfaces in food: Structure and mechanical properties. *Trends in Food Science & Technology, 37*(1), 59–71.
Schindelin, J., Arganda-Carreras, I., Frise, E., Kaynig, V., Longair, M., Pietzsch, T., Preibisch, S., Rueden, C., Saalfeld, S., & Schmid, B. (2012). Fiji: An open-source platform for biological-image analysis. *Nature Methods, 9*(7), 676–682.
Sun, Y., Zhong, M., Wu, L., Huang, Y., Li, Y., & Qi, B. (2022). Effects of ultrasound-assisted salt (NaCl) extraction method on the structural and functional properties of Oleosin. *Food Chemistry, 372*, Article 131238.
Tzen, J., & Huang, A. (1992). Surface structure and properties of plant seed oil bodies. *Journal of Cell Biology, 117*(2), 327–335.
Tzen, J., Lie, G., & Huang, A. (1992). Characterization of the charged components and their topology on the surface of plant seed oil bodies. *Journal of Biological Chemistry, 267*(22), 15626–15634.

Vargo, K. B., Parthasarathy, R., & Hammer, D. A. (2012). Self-assembly of tunable protein suprastructures from recombinant oleosin. *Proceedings of the National Academy of Sciences, 109*(29), 11657–11662.

Wahlroos, T., Soukka, J., Denesyuk, A., & Susi, P. (2015). Amino-terminus of oleosin protein defines the size of oil bodies-topological model of oleosin-oil body complex. *Journal of Plant Biochemistry & Physiology, 3*, 155.

Weiss, J., & Zhang, H. (2020). Recent advances in the composition, extraction and food applications of plant-derived oleosomes. *Trends in Food Science & Technology, 106*, 322–332.

Yang, J., Berton-Carabin, C. C., Nikiforidis, C. V., van der Linden, E., & Sagis, L. M. (2022). Competition of rapeseed proteins and oleosomes for the air-water interface and its effect on the foaming properties of protein-oleosome mixtures. *Food Hydrocolloids, 122*, Article 107078.

Zaaboul, F., Raza, H., Lazraq, A., Deng, B., Cao, C., & Liu, Y. F. (2018). Chemical composition, physical properties, and the oxidative stability of oil bodies extracted from Argania spinosa. *Journal of the American Oil Chemists' Society, 95*(4), 485–495.

Zhou, H.-X., & Pang, X. (2018). Electrostatic interactions in protein structure, folding, binding, and condensation. *Chemical Reviews, 118*(4), 1691–1741.